Unique Difference in Transition Temperature of Two Similar Fluorinated Side Chain Polymers Forming HexaticSmectic phase: Poly{2-(Perfluorooctyl) Ethyl Acrylate} and Poly{2-(Perfluo…

ARTICLE *in* MACROMOLECULES · JUNE 2014

Impact Factor: 5.8 · DOI: 10.1021/ma500503z

7 AUTHORS, INCLUDING:

A. Meskini
Claude Bernard University Lyon 1
6 PUBLICATIONS **56** CITATIONS
SEE PROFILE

Mustapha Raihane
Faculty of Sciences and Technologies-Cadi Ay…
66 PUBLICATIONS **365** CITATIONS
SEE PROFILE

Atsushi Takahara
Kyushu University
487 PUBLICATIONS **8,480** CITATIONS
SEE PROFILE

Bruno Ameduri
Ecole Nationale Supérieure de Chimie de Mon…
344 PUBLICATIONS **5,076** CITATIONS
SEE PROFILE

Macromolecules

Article

pubs.acs.org/Macromolecules

Unique Difference in Transition Temperature of Two Similar Fluorinated Side Chain Polymers Forming Hexatic Smectic Phase: Poly{2-(perfluorooctyl)ethyl acrylate} and Poly{2-(perfluorooctyl)ethyl vinyl ether}

Ryohei Ishige,[†] Takamichi Shinohara,[‡] Kevin L. White,[†,§] Ahmed Meskini,[∥] Mustapha Raihane,[∥] Atsushi Takahara,*[,†,‡,§,⊥] and Bruno Ameduri[#]

[†]Institute for Materials Chemistry and Engineering, [‡]Graduate School of Engineering, and [§]International Institute for Carbon-Neutral Energy Research (I[2]CNER), Kyushu University, 744 Motooka, Nishi-ku, Fukuoka 819-0395, Japan

[∥]Organometallic and Macromolecular Chemistry-Composite Materials Laboratory − Cadi Ayyad University-Faculté des Sciences et Techniques, Avenue Abdelkrim Khattabi, BP 549, 40000 Marrakech, Morocco

[⊥]Exploratory Research for Advanced Technology (ERATO), Takahara Soft Interfaces Project, Japan Science and Technology Agency (JST), 744 Motooka, Nishi-ku, Fukuoka 819-0395, Japan

[#]Engineering and Macromolecular Architectures, Institut Charles Gerhardt, UMR (CNRS) 5253, Ecole Nationale Supérieure de Chimie de Montpellier, 8 Rue Ecole Normale, 34296 Montpellier Cedex 5, France

Supporting Information

ABSTRACT: The surface properties of comb-shaped polymers with perfluorooctyl ethyl side-chains are strongly related to the ordered structure of the side-chains at the surface. In this work, the thermal behavior, liquid-crystalline structure, and functional group orientation of comb-shaped polymers containing perfluorooctyl side-chains with poly(acrylate) (PFA-C_8) and poly(vinyl ether) (PFAVE8) backbones are discussed based on DSC, synchrotron-source X-ray diffraction, and FTIR measurements. Despite the similar tilted hexatic smectic structures and packing entropies, the isotropization temperature, T_i, of the PFA-C_8 is significantly higher than the PFAVE8. Detailed characterization of the conformation, alignment, and organization of the perfluorooctyl side-chains indicate that the difference in T_i is related to the configuration of side-chains and interactions between the carbonyl groups along the acrylate backbone. The present findings show that the type of the linkage between the polymer backbone and fluorinated side-chain mesogens affects the conformation and plays an important role in determining thermal behavior.

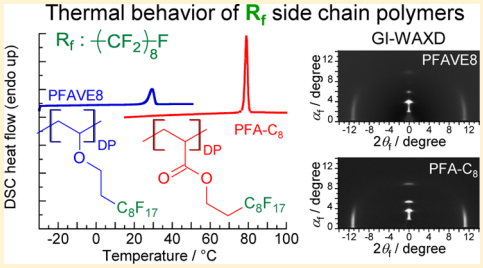

1. INTRODUCTION

It is well-known that long *n*-alkyl side-chains in comb-shaped polymers form similar crystal phases to the corresponding normal paraffin.[1] The *n*-alkyl side-chains in comb-shaped polymers are easily anchored perpendicular to the interface, which may be a solid/air,[2] liquid/liquid-crystal,[3,4] or liquid/air interface,[5−7] and retain ordered structure at higher temperature than the bulk. Owing to the side-chain ordering at the surface, such comb-shaped polymers show good hydrophobicity comparable to self-assembled monolayers of the corresponding *n*-alkyl chains.[1,5] For fabrication of hydrophobic surfaces, perfluoroalkyl chains have a better potential because the chains are more rigid than *n*-alkyl chains,[8] and remain ordered in the bulk and at the surface at higher temperature than *n*-alkyl chains with the same length.[1,8−13] In particular, comb-shaped polymers with perfluorooctyl (−C_8F_{17}, R_f) side chains[9−13] show excellent hydrophobicity[14] that is related to the ordered arrangement of perfluoroalkyl groups at the outermost layer. Previous wide-angle X-ray diffraction (WAXD) measurements of powder samples have shown that poly(acrylate) with 2-(perfluorooctyl) ethyl side chains (abbreviated here as PFA-C_8) forms a smectic-*B* (S_B) phase,[15] which is a hexatic liquid crystal.[16−18] In this S_B phase model, the rigid R_f side chains are mesogens and segregate from the polymer backbone to form a bilayer lamellar structure with 2-dimensional (2D) hexagonal order.

Honda et al. investigated the structure of PFA-C_8 thin films deposited on a silicon wafer using 1-dimensional (1D) grazing-incidence WAXD (GI-WAXD) and X-ray photoelectron spectroscopy.[19−21] The results revealed that a bilayer of R_f chains forms almost parallel to the surface and that the CF_3 groups at the side-chain ends are concentrated at the outermost surface. The bilayer arrangement of the side-chains at the surface is the same as that formed in the bulk. The low surface free energy of the polymer was attributed to the ordered smectic arrangement, which is similar to that observed with the long *n*-alkyl side-chain polymers.[19,20] The importance of ordered structure was clearly

Received: March 8, 2014
Revised: May 17, 2014
Published: June 4, 2014

demonstrated by Honda et al.,[21] who reported that a series of polymers with the same poly(acrylate) backbone and short perfluoroalkyl side-chains with fewer than 7 carbon atoms (PFA-C_n, $n < 7$) show amorphous structure and inferior surface properties. To obtain desired surface properties, it is important to understand and control the ordered structure of the fluorinated side-chains. However, clear 2D WAXD patterns of well-oriented samples of these polymers have not been previously obtained because of difficulties in the preparation of oriented samples with sufficient size for measurement.

In this study, we have investigated the ordered structure, development mechanism, phase transition behavior, and functional group orientation of PFA-C_8 and a corresponding polymer with poly(vinyl ether) backbone, abbreviated as PFAVE8. The ordered structure and mechanism of development were studied using synchrotron-source radiation for high resolution powder WAXD, microbeam 2D WAXD of thick film samples, and 2D GI-WAXD of thin films deposited on a silicon wafer. The phase transition behavior was investigated using differential scanning calorimetry (DSC). The orientation of functional groups (ethylene spacer and carbonyl group) was probed with Fourier transform infrared spectroscopy (FTIR) of thin films on a KBr plate. The results provide insights into the relationship between the phase transition behavior and molecular configuration in the ordered structure. The present findings show that in comb-shaped polymers with R_f mesogenic side-chains, the type of bonds connecting the spacer and backbone does not significantly influence the transition entropy and hexatic structure formation, but strongly affects the transition enthalpy and transition temperature.

2. EXPERIMENTAL SECTION

2.1. Materials. The synthesis of the fluorinated side-chain polymers poly{2-(perfluorooctyl) ethyl acrylate}[22] (PFA-C_8) and poly{2-(perfluorooctyl) vinyl ether}[23,24] (PFAVE8) has been reported elsewhere. The chemical structure of PFA-C_8 and PFAVE8 is shown in Figure 1. All procedures involving compounds containing C_8F_{17}, e.g.,

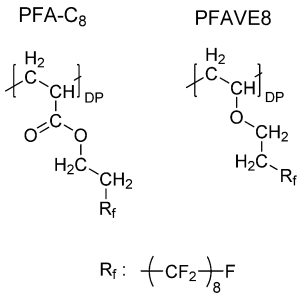

Figure 1. Chemical structure of poly{2-(perfluorooctyl) ethyl acrylate} (PFA-C_8) and poly{2-(perfluorooctyl) ethyl vinyl ether} (PFAVE8).

perfluorooctanic acid (PFOA), perfluorooctanesulfonate (PFOS), etc., should be conducted under a hood (Caution!) due to the known bioaccumulation risk.[25] AK-225 (Asahi Glass Co., Tokyo, Japan), a fluorine containing solvent (mixture of 1,1-dichloro-2,2,3,3,3-pentafluoropropane and 1,3-dichloro-1,1,2,2,3-pentafluoropropane), was used as received to prepare the polymer solution for spin-coating and dip-coating processes.

2.2. Measurements. DSC measurements were performed with a PerkinElmer Diamond DSC (PerkinElmer Inc., Waltham, MA) under nitrogen flow at scanning rate of 10 °C min^{-1}. FTIR measurements of nonoriented powder samples and perpendicularly oriented samples were conducted with an AutoImage micro-FTIR microscope system (PerkinElmer Inc., Waltham, MA) with 4 cm^{-1} resolution. The analysis area was 100 × 100 μm^2. The oriented thin film sample was dip-coated on a KBr plate from 0.5 wt % polymer solution in AK-225. The films were subsequently annealed at T_i − 5 °C for 12 h, where T_i is the isotropization temperature determined from DSC. KBr pellets of the nonoriented powder samples annealed in the same way were prepared using the Tablet Master fixture (JASCO Co., Tokyo, Japan).

High-resolution powder WAXD measurements were done at the BL02B2 beamline in the SPring-8 synchrotron research facility (Japan Synchrotron Radiation Research Institute, Hyogo, Japan), using a Debye−Scherrer camera. The size of the imaging plate (IP) detector was 200 × 400 mm^2 with pixel size of 100 × 100 μm^2. The distance from the sample to detector (radius of the camera) was 286.5 mm and the X-ray wavelength was 0.10 nm. The powder sample was sealed in a 0.7φ Mark tube of Lindemann glass (Hilgenberg Co., Malsfeld, Germany) and the temperature was controlled using a high temperature nitrogen gas flow system equipped at the beamline. The observed intensity $I_{obs}(\theta)$ was Lorentz-corrected. For this beamline, the X-ray polarization factor is 1 and the integrated intensity is proportional to $I_{obs}(\theta)$ sin θ sin 2θ,[26] where θ is the Bragg scattering angle.

Microbeam WAXD measurements of PFA-C_8 were carried out at the BL40XU beamline in SPring-8. The wavelength of the X-ray beam was 0.10 nm, the beam size half-width was 2.9 × 3.5 μm (height × width), and the camera radius was 112 mm. The length was calibrated using CeO_2 standard. Diffraction patterns were recorded with an X-ray image intensifier (Hamamatsu Photonics, V5445P) and fast CCD camera (Hamamatsu Photonics, C4880−80).

2D GI-WAXD measurements of PFA-C_8 and PFAVE8 were performed at the BL03XU beamline in the SPring-8 facility. The wavelength of the X-ray beam was 0.10 nm and the camera length was 475 mm for PFA-C_8 and 452 mm for PFAVE8. The camera length was calibrated using silver behenate standard. The diffraction images were captured using a 3000 × 3000 pixel IP with pixel size of 100 × 100 μm^2 (Fujifilm Co., Tokyo, Japan). The IP was equipped on a R-AXIS IV++ system (Rigaku Co., Tokyo, Japan). For GI-WAXD measurements, thin films were prepared on disk-shaped silicon (111) wafers with 1 in. diameter and 3 mm thickness. The thin films were prepared by spin-coating at 2000 rpm for 30 s from 1.0 wt % polymer solution in AK-225. The deposited films were subsequently annealed using the same conditions as for FTIR measurements (T_i − 5 °C for 12 h). The samples were mounted in a homemade vacuum cell with polyimide (KAPTON) window to avoid sample oxidation and introduction of scattering effects from air. The detailed configuration of this beamline is reported elsewhere.[27] All X-ray and FTIR measurements were conducted at room temperature (27 °C).

3. RESULTS AND DISCUSSION

3.1. Phase Transition Behavior. DSC thermograms of PFA-C_8 and PFAVE8 obtained during second heating and cooling cycles are shown in Figure 2. During heating, an endothermic peak was observed for both polymers. The isotropization temperature, T_i (temperature at the peak of the endotherm during

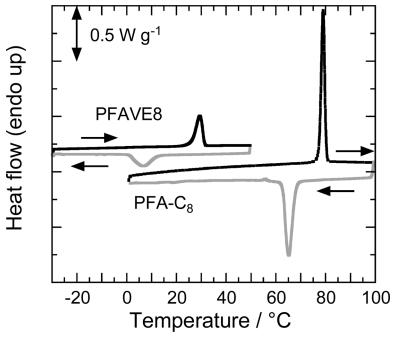

Figure 2. DSC thermograms of PFA-C_8 and PFAVE8 during second heating and cooling cycles, measured with scanning rate of 10 °C min^{-1} under N_2 flow.

dx.doi.org/10.1021/ma500503z | Macromolecules 2014, 47, 3860−3870

heating), transition enthalpy, ΔH, and transition entropy, ΔS, were 79 °C, 7.4 kJ mol^{-1}, and 21 J mol^{-1} K^{-1} for PFA-C_8 and 29.5 °C, 5.3 kJ mol^{-1}, and 18 J mol^{-1} K^{-1} for PFAVE8, respectively. The isotropization temperature of PFA-C_8 is nearly 50 °C greater than that of PFAVE8. As discussed in sections 3.2 and 3.4, the two polymers form similar hexatic smectic phases, which suggests that the packing entropy (translational entropy) of the two polymers will be nearly the same and is consistent with the small difference in ΔS observed with DSC measurements. The ratio of isotropization temperatures, T_1/T_2, should therefore be nearly equal to the ratio of the transition enthalpies (i.e., $T_1/T_2 = \Delta H_1\Delta S_2/\Delta H_2\Delta S_1 \approx \Delta H_1/\Delta H_2$). It should be noted that although the melting point of poly(*n*-alkyl acrylate) is slightly lower than that of poly(*n*-alkyl vinyl ether),[1] the T_i of PFA-C_8 is significantly higher than that of PFAVE8. The significant difference in T_i, and opposing tendency of melting temperature, cannot be explained based solely on differences in primary structure. The significant difference in T_i must then be related to differences in enthalpy, which may potentially be attributed to interactions between polar groups, provided that the densities of the two polymers are comparable. This conjecture is explored in detail in the following sections.

Large differences in T_i related to ΔH may be an inherent feature of highly ordered smectic phases, such as the hexatic phase shown in the following sections. In the case of less ordered smectic phases, e.g., smectic-*A* phase, ΔS is small and may depend on the conformation of backbone and spacer chains, as well as the layer order related to the packing entropy. As a result, T_i should depend on both ΔH and ΔS. Omenat and co-workers[28] reported that side-chain liquid-crystalline poly(methacrylate) and poly(vinyl ether) with the same backbone and spacer chain structure show nearly the same smectic-*A*-to-isotropic phase transition temperature, even though ΔH of the poly(methacrylate) (1.5 kJ mol^{-1}) was 2.3 times larger than ΔH of the poly(vinyl ether) (0.64 kJ mol^{-1}). In these less ordered smectic phases, the difference in ΔS between the two polymers was 2.4 J mol^{-1} K^{-1}, which is large compared to the absolute value of ΔS for each polymer (4.1 J mol^{-1} K^{-1} and 1.7 J mol^{-1} K^{-1} for the poly(methacrylate) and poly(vinyl ether), respectively), and offsets the difference in ΔH, resulting in similar T_i. We similarly reported that the alternating copolymer of vinylidene cyanide and perfluorooctyl ethyl vinyl ether had significantly higher T_i (178 °C) than the PFAVE8 homopolymer (29.5 °C).[29] However, in this system it is difficult to directly relate the large difference in T_i to ΔH because the alternating copolymer forms a less-ordered smectic phase with much smaller ΔS (3.9 J mol^{-1} K^{-1}) than the PFAVE8 homopolymer (18 J mol^{-1} K^{-1}). For the PFA-C_8 and PFAVE8 reported here, the magnitude of ΔS is similar despite the differences in primary structure of the backbone, which provides a useful basis for comparative study of the thermodynamic factors influencing phase stability in highly ordered liquid crystals.

3.2. Ordered Structure of the Powder Samples. High-resolution WAXD profiles were obtained at 27 °C for both polymers. The integrated intensity (Lorentz-corrected) profiles are shown in Figure 3a,b. In the small angle region, diffraction peaks were observed at q = 1.98, 3.91, 5.85, and 9.74 nm^{-1} for the PFA-C_8 and q = 2.12, 4.23, 6.35, 8.40, and 10.06 nm^{-1} for the PFAVE8. The peaks appear at the same intervals for both polymers. The reciprocal spacing of the most inner diffraction peak is 3.18 nm for the PFA-C_8 and 2.96 nm for the PFAVE8, which corresponds to the length of the bilayer formed by one pair of R_f side chains. The spacing of the diffraction peaks

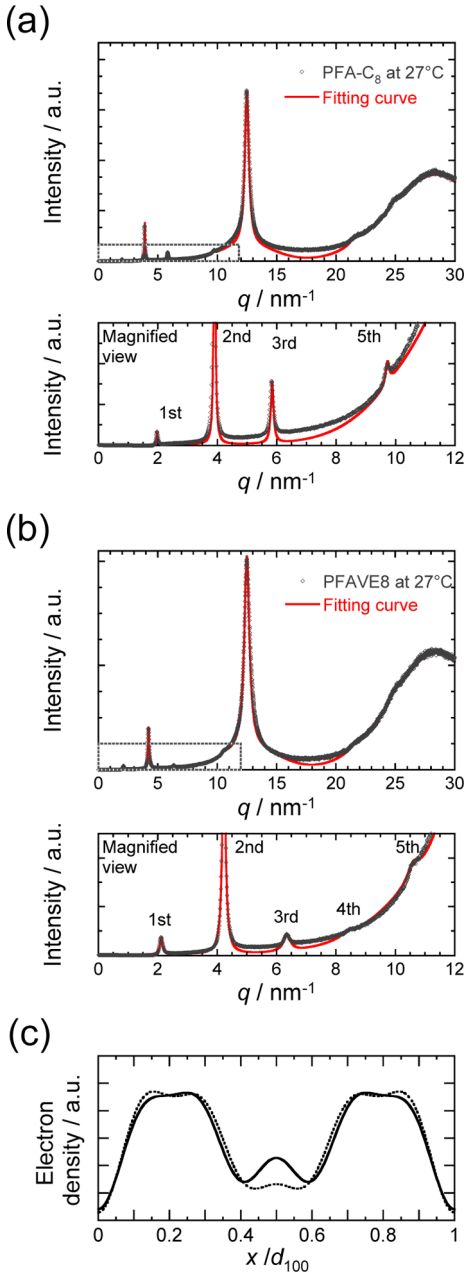

Figure 3. Lorentz-corrected intensity profiles of high resolution powder WAXD measurements obtained for (a) PFA-C_8 and (b) PFAVE8 at 27 °C. Multiple diffraction peaks were separated using Lorentz functions (solid line). Magnified views from 0 to 12 nm^{-1} (indicated by dotted box in each upper graph) shown below intensity profiles in a and b. (c) Most probable electron density profiles in layer normal direction, x, for PFA-C_8 (solid line) and PFAVE8 (dotted line), calculated by Fourier reconstruction of the h00 diffractions.

corresponds to the first, second, third, and fifth order diffractions for PFA-C_8, and the first, second, third, fourth, and fifth layer diffractions for PFAVE8.[16−18,29] The WAXD profiles of PFAVE8 display the fourth order layer diffraction, whereas the PFA-C_8 does not. The WAXD peaks corresponding to the smectic structure of PFA-C_8 do not show clear temperature dependence from 27 to 70 °C (raw powder WAXD (nonintegrated) profiles for PFA-C_8 from 27 to 85 °C are provided in the Supporting Information). Therefore, the results of PFA-C_8 and PFAVE8 at 27 °C can be directly compared, despite the large difference in T_i.

dx.doi.org/10.1021/ma500503z | Macromolecules 2014, 47, 3860−3870

In the outer region of $q > 11$ nm^{-1}, the PFA-C_8 shows one strong peak at 12.4 nm^{-1} and two very weak peaks at 21.5 nm^{-1} and 24.7 nm^{-1}. The PFAVE8 exhibits peaks with similar intensities at 12.5, 21.7, and 25.0 nm^{-1}. The peaks are attributed to structure corresponding to the lateral separation of the R_f groups. The ratio of q-values in the outer region diffraction peaks are $1:3^{1/2}:2$ for both polymers, which indicates that the R_f groups are arranged in a 2D hexagonal lattice and therefore constitute a hexatic smectic phase.[17,18] The full-width at half maxima of the peaks are almost the same in the two samples, which suggests that the degree of positional order of the hexatic phases is almost the same. This point is discussed in greater detail in section 3.4.

One can easily envisage that the structural differences between the PFA-C_8 and PFAVE8 responsible for the missing fourth order layer diffraction peak in the PFA-C_8 will be sufficient to account for the large difference in T_i. To identify the structural differences in greater detail, electron density profiles, $\rho(x)$, in the layer normal direction, x, were calculated using Fourier reconstruction.[12,13,30,31] The electron density profiles were normalized by the number of observed diffraction peaks for each polymer. If $\rho(x)$ is centrosymmetric, as for smectic layers,[12,13] the structure factor in the layer normal direction, $F(q_h)$, is a real number equal to the square root of the intensity $I(q_h)$ at $q_h = h/d$

$$F(h/d) = \pm\sqrt{I(h/d)} \tag{1}$$

where h and d are the order of diffraction and spacing of the smectic layer, respectively. The electron density profile in the layer normal direction may then be expressed as

$$\rho(x) = \sum_{h=-\infty}^{\infty} \pm\sqrt{I(h/d)}\ \exp(2\pi i h(x/d)) \tag{2}$$

Details of the derivation are included in the Supporting Information.

The most probable electron density profiles for the bilayer structure were calculated from eq 2 and are shown in Figure 3c. The signs of $I(h/d)^{1/2}$ used for the profiles are +, −, −, − for PFA-C_8 and +, −, −, −, − for PFAVE8, in order of increasing h index from the lowest to highest order diffraction peaks in the small angle region. The profiles obtained from both polymers show very similar bimodal peaks that correspond to the high electron density of the R_f groups. However, the density around the backbone chain position is slightly different. The electron density of the PFA-C_8 backbone is larger than that of the PFAVE8, which indicates that the heteroatom, i.e., the oxygen atom, is more densely concentrated in the sublayer between the R_f layers for the PFA-C_8. This result implies that the polar carbonyl groups can easily interact in the sublayer for the PFA-C_8. The orientation of the dimethylene spacers for both polymers, as well as the carbonyl group for the PFA-C_8, is discussed in sections 3.5 and 3.6.

3.3. Orientation Distribution in PFA-C_8 Thick Film. For PFA-C_8 thin films (~100 nm thickness), we previously reported that the layer structure is aligned perpendicular to the surface.[20] For thick films, it is important to determine the correlation length of the layer orientation to ensure uniformity of orientation in the thickness direction. Uniformity is essential for meaningful analysis of thin films using techniques such as GI-WAXD and FTIR, which are reported in section 3.4 and 3.5. Previously, we were unable to assess the degree of uniformity for thick films because the X-ray beam size in lab-scale experiments is too large to obtain sufficient spatial resolution. Here, we studied the orientation distribution in thick films of PFA-C_8 using synchrotron-source microbeam WAXD.[32] The film had width of about 1700 μm and thickness of 150 μm, and was tilted 2.5° from the direction of the X-ray beam (Figure 4a,b). To avoid shear-flow induced orientation, the films were prepared by cooling from the isotropic melt on a Teflon sheet *in vacuo* without pressing. The free-standing film was then peeled from the sheet.

The X-ray beam was irradiated perpendicular to the edge plane of the film for 1.0 s. Diffraction patterns were obtained at multiple positions beginning from the top surface (air-sample interface), and moving the sample stepwise in the thickness direction, x, at intervals of 5 μm (Figure 4e). The bottom surface is designated as the interface between the Teflon sheet and free-standing polymer film prior to peeling.

Near the top surface, from $x = 55$ to 105 μm, and the bottom surface, from $x = 230$ to 285 μm, oriented 2D WAXD patterns were observed (Figure 4b). Debye-Scherrer rings characteristic of unoriented structure are observed in the film interior. The diffraction patterns show that the smectic layer normal is oriented nearly parallel to the thickness direction at the top and bottom surfaces, and that in the film interior, there is negligible orientation. The degree of orientation was estimated by the orientational order parameter, S, given by

$$S = \frac{1}{2}(3\langle\cos^2\chi\rangle - 1),$$
$$\langle\cos^2\chi\rangle = \frac{\int_0^\pi \cos^2\chi I(\chi)|\sin\chi|\,d\chi}{\int_0^\pi I(\chi)|\sin\chi|\,d\chi} \tag{3}$$

where $I(\chi)$ is the intensity distribution function of the layer diffraction in the direction of angle χ, and χ is the angle between the layer normal and the surface normal. The angle χ satisfies $\cos\chi\cdot\cos\theta = \cos\beta$, where β is the azimuthal angle in the WAXD image and θ is the Bragg angle.[33] The angle β is equal to 0 at the meridian. The orientational order parameter is large and nearly the same at the top ($S \sim 0.95$) and bottom surfaces ($S \sim 0.89$), and nearly zero in the film interior (Figure 4e).

The results show that the film may be divided into two regions: an oriented region at the top and bottom surfaces, and a non-oriented region in the film interior. Since the scattering intensity is proportional to the irradiated volume, the volume occupied by each region, V_i ($i = 1, 2$), may be estimated from the integrated intensity,[33] Q_i, which is given by

$$Q_i = \int_0^\pi I_i(\chi)|\sin\chi|\,d\chi, \qquad i = 1 \text{ or } 2 \tag{4}$$

where the indices 1 and 2 correspond to the oriented and non-oriented regions of the film, respectively. The values of Q_1 and Q_2 for the PFA-C_8 thick film through the thickness direction, x, are shown in Figure 4d. Near the surface and interface regions, Q_1 is nearly constant and independent of position, while Q_2 increases with x due to the tilting of the film. The volume of each region is given by the thickness of the ordered region, t, and the total irradiated area (3.5 μm width by 2.9 μm height), and may be expressed as $V_1 = 3.5 \times t^2/\tan 2.5°$ and $V_2 = 3.5/2 \times (2.9 - t)^2/\tan 2.5°$. The correlation length of layer orientation, t, was estimated from the ratio of Q_1/Q_2 to be about 1.4 μm at the top surface and 1.2 μm at the bottom surface.

The observed orientation distribution is a consequence of the growth mechanism for the smectic layer structure. Based on X-ray reflectivity measurements of 12CB, Ocko et al. showed that a smectic-*A*-like layer structure develops by discrete steps from the outermost surface toward the interior prior to an isotropic to

dx.doi.org/10.1021/ma500503z | *Macromolecules* 2014, 47, 3860−3870

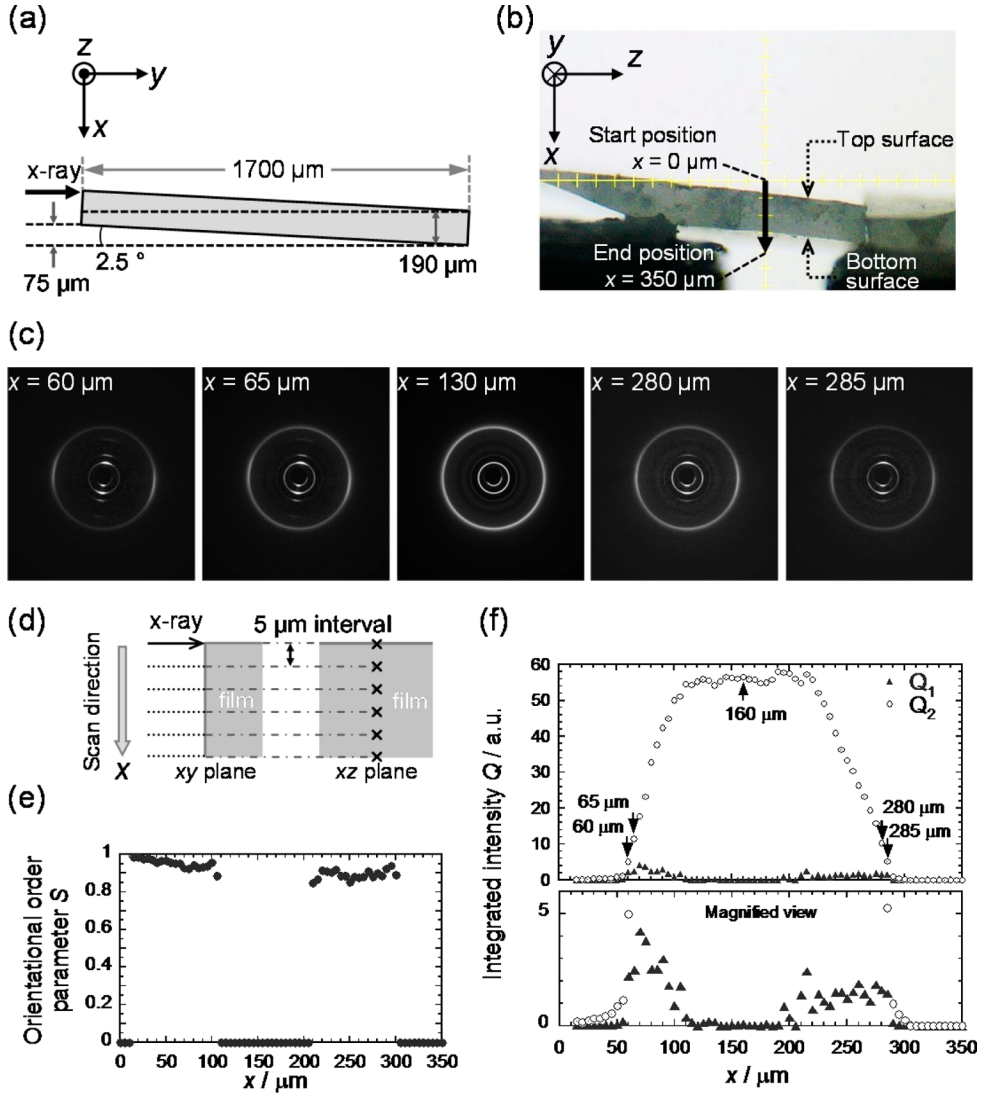

Figure 4. (a) Schematic showing geometry of microbeam WAXD measurement of PFA-C_8 thick film. (b) Microscope image of thick film; Cartesian coordinate system (*xyz*) inset. X-ray incident beam is parallel to the *y*-axis and the normal of the surface is near the *x*-axis. (c) WAXD images taken at different positions through thickness of film. (d) Schematic representing X-ray direction along *x*-axis with respect to *xy* and *xz* planes. (e) Orientational order parameter plotted as a function of *x*. (f) Integrated intensities, Q_1 in the oriented region (closed triangles) and Q_2 in the nonoriented region (open circles), plotted with measurement position along sample thickness direction, *x*.

smectic-*A* phase transition in the bulk.[34] Gautam similarly reported that *n*-alkyl side-chains in comb-shaped polymers show crystalline order at the surface at temperatures greater than the bulk melting temperature.[6] It is natural to consider that the growth of the smectic layer structure of the PFA-C_8 thick film proceeds in a similar way. The results suggest that the oriented layer initiated at the surface penetrates about 1.4 μm toward the interior of the film. This mechanism should depend on the type of mesogen, i.e., the surface free energy of the mesogen rather than the backbone structure, because surface adsorption of the mesogen will dominate the layering transition at the surface.[34] Therefore, the PFAVE8 should show the same mechanism of crystal growth as the PFA-C_8 because they have the same R_f mesogens. The results show that in the oriented region, the layer orientation is uniform in the thickness direction and there is no significant gradient in the orientation distribution (Figure 4f). The orientational homogeneity in the surface region observed here is an implicit assumption of the structural models used in the following sections.

3.4. Structural Analysis of Highly Oriented 2D GI-WAXD Patterns of Thin Films. 2D GI-WAXD oriented patterns were obtained for the PFA-C_8 and PFAVE8 thin films to determine the correlation between neighboring layers and orientation of R_f groups. Spin-coated thin films with thickness of about 100 nm were deposited on a Si wafer and used for the GI-WAXD measurements. The critical angle, α_c, of the X-ray with energy of 12.4 keV is about 0.12° for the fluorinated polymers and 0.14° for the Si substrate. Measurements were performed with incident angles, α_i, of 0.08° and 0.16°. For α_i = 0.08° < 0.12°, the X-rays can exist only as evanescent waves parallel to the surface and the penetration depth is limited to about 1 nm. When α_i = 0.16° > 0.12°, the X-rays can penetrate the film down to the substrate. As a result, diffractions at α_i = 0.08° contain information limited to the outermost surface region, while those at α_i = 0.16° are sensitive to the structure throughout the film.

Well-oriented 2D GI-WAXD patterns similar to the microbeam WAXD patterns were obtained for both incident angles

dx.doi.org/10.1021/ma500503z | *Macromolecules* 2014, 47, 3860−3870

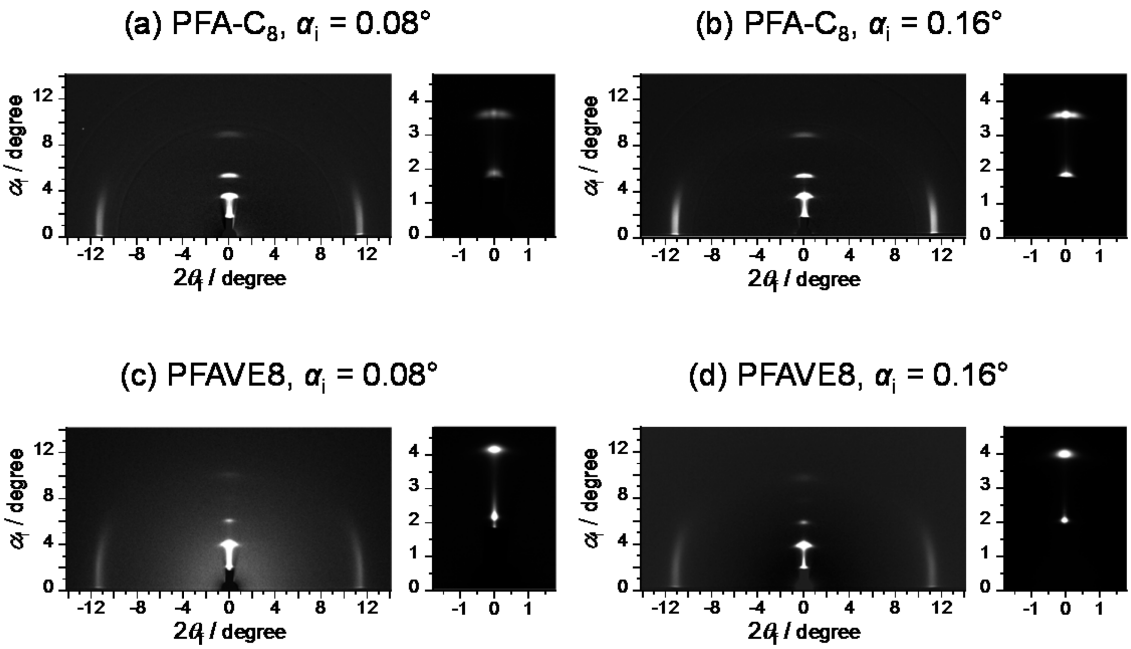

Figure 5. GI-WAXD patterns of PFA-C_8 (a, b) and PFAVE8 (c, d) taken with X-ray incident angles, α_i of 0.08° (a, c) and 0.16° (b, d). First and second order (h00) diffractions are magnified on right of each pattern.

and are shown in Figure 5a,b. The patterns for both polymers are similar. Layer diffractions (h00 diffractions) were observed along the meridian and the 010 (001) diffractions appear as long, diffuse streaks in the vertical direction. Slight differences in the second order layer diffraction are present. For the PFA-C_8, the second order diffraction peak is characteristically split into three spots around the meridian (Figure 5a,b), whereas the PFAVE8 shows only one spot (Figure 5c,d). Herein, the averaged lattice parameter a is defined in the long-axis direction of the R_f and the lattice parameter c is defined in the polymer-chain direction. Both polymers show a 2D hexagonal lattice that lies in the plane perpendicular to **a** (Figure 6a). The geometry of the layer, (h00),

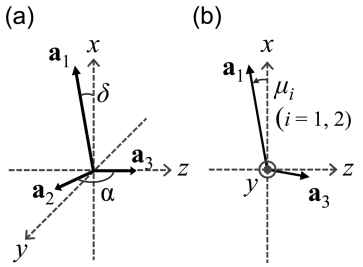

Figure 6. (a) Schematic view of oblique lattice vectors $\mathbf{a}_1$, $\mathbf{a}_2$, $\mathbf{a}_3$, and tilt angle δ, when orientation angle $\mu_i = \delta$. The lattice vectors $\mathbf{a}_2$ and $\mathbf{a}_3$ lie on the yz plane. (b) Model of orientation of $\mathbf{a}_1$ in region i (i = 1, 2) for orientation angle, μ_i. The Cartesian x- and z-axes are defined in the vertical (out-of-plane) and horizontal (in-plane) directions, respectively. Incident X-ray is parallel to the y-axis. The angle between the x-axis and the orientation direction of the $\mathbf{a}_1$ vector in region i is defined as μ_i.

and lateral, (0k0) and (00l), diffractions implies that the polymers form a tilted hexatic phase and that at least two different orientations coexist in the PFA-C_8 film. In the following paragraph, the same model used for the PFA-C_8 will be used to analyze the PFAVE8 GI-WAXD patterns.

The reflectivity of the interface between the substrate and the sample may be neglected for the experimental configuration used here (more detailed discussion provided in the Supporting Information).[35,36] As a result, except for the small angle region around the equator, the Born approximation can be applied to the GI-WAXD patterns taken with α_i = 0.08° and 0.16° in a similar manner to typical transmission WAXD patterns. To evaluate the tilt angle, δ, and correlation between neighboring layers, we calculated the intensity profile using the paracrystal model[37−40] of an oblique lattice with infinite grain size (Figure 6a). The model assumes that two populations of orientation coexist: in region 1, the layer normal direction is aligned perpendicular to the surface, and in region 2, the layer normal direction is tilted by μ_2 (Figure 6b). The orientation distribution function $D(\mu)$ of the paracrystals is given by

$$D(\mu) = \sum_{i=1}^{2} f_i \frac{1}{\sqrt{2\pi}\,\sigma_i} \exp\left(\frac{-(\mu - \mu_i)^2}{2\sigma_i^2}\right) \quad (5)$$

where μ is the orientation angle, i is an index for region of orientation defined above, μ_i is the angle between the averaged direction of the **a** vector and the x-axis, σ_i is the standard deviation of μ_i, and f_i is the volume fraction of region i. The orientation angle is defined such that μ = 0 along the x-axis (vertical direction). The intensity, $I(\mathbf{q})$, of a single paracrystal is given as follows

$$I(\mathbf{q}) \propto \langle F(\mathbf{q})^2 \rangle - \langle F(\mathbf{q}) \rangle^2 + \langle F(\mathbf{q}) \rangle^2 Z(\mathbf{q}) \cong \langle F(\mathbf{q}) \rangle^2 Z(\mathbf{q}) \quad (6)$$

where $Z(\mathbf{q})$ is the lattice factor and $F(\mathbf{q})$ is the structure factor of the unit cell. In eq 6, the lattice factor $Z(\mathbf{q})$ is defined as the product of the three k-th order lattice factors, $Z_k(\mathbf{q})$ (k = 1, 2, 3), which were calculated from eq 7:

$$Z_k(\mathbf{q}) = \frac{1 - |F_k(\mathbf{q})|^2}{1 + |F_k(\mathbf{q})|^2 - 2|F_k(\mathbf{q})|\cos(\mathbf{q}\cdot\langle \mathbf{a}_k \rangle)},$$
$$\langle \mathbf{a}_1 \rangle = \mathbf{a}, \quad \langle \mathbf{a}_2 \rangle = \mathbf{b}, \quad \langle \mathbf{a}_3 \rangle = \mathbf{c} \quad (7a)$$

dx.doi.org/10.1021/ma500503z | Macromolecules 2014, 47, 3860−3870

$$|F_k(\mathbf{q})| = \iiint_V h_k(\mathbf{x}) \exp(\mathbf{q}\cdot(\mathbf{r} - \langle \mathbf{a}_k \rangle))\, d\mathbf{x} = \prod_{j=1}^{3} \exp\left\{-\frac{1}{2}(g_{kj}{}^2(\mathbf{q}\cdot\langle \mathbf{a}_j \rangle)^2)\right\} \quad (7b)$$

$$h_k(\mathbf{x}) = \prod_{j=1}^{3} h_{kj}(x_j), \quad j = 1, 2, 3 \quad (7c)$$

$$h_{kj}(x_j) = \left(\frac{1}{\sqrt{2\pi}\, g_{kj}}\right) \exp\left(\frac{(x_j - \delta_{kj})^2}{2g_{kj}{}^2}\right) \quad (7d)$$

$$g_{kj}{}^2 = \int_{-\infty}^{\infty} h_{kj}(x_j)(x_j - \delta_{kj})^2\, dx_j \quad (7e)$$

The brackets in eq 7a represent statistically averaged quantities. In eq 7c, x_1, x_2, and x_3 are the components of the real space vector $\mathbf{x}$ whose basis vectors are the lattice vectors $\mathbf{a}$, $\mathbf{b}$, $\mathbf{c}$ (i.e., $\mathbf{x} = x_1\mathbf{a} + x_2\mathbf{b} + x_3\mathbf{c}$) and g_{kj} corresponds to normalized standard deviation of the x_j component of $\mathbf{a}_k$. In eq 7d, δ_{kj} is the Kronecker delta function and $h_k(\mathbf{x})$ is a distribution function of the $\mathbf{a}_k$ vector with second-kind disorder. The above eqs 5−7 were used to simulate the 2D-WAXD patterns (more detail provided in the Supporting Information).

The calculated 2D WAXD patterns and line intensity profiles are shown in Figure 7. The lattice parameters used for the calculations are listed in Table 1. The parameters in the bulk and surface regions are similar for both polymers, except for the orientation angle μ_i. For the PFA-C_8 and PFAVE8, the tilt angle δ is about 11° and 16°, and the orientation angle (μ_1, μ_2) is (11°, 5°) and (16°, 10°), respectively, for both surface and interior regions. For both polymers, the orientation angle μ_1 is the same as the tilt angle and, on average, the layer normal, $\mathbf{n}$, is aligned perpendicular to the surface in region 1, and tilts by 6° ($= \delta - \mu_i$) in region 2 (Figure 8a,b). The volume fraction of oriented regions, f_1 and f_2, are almost the same and the degree of orientation is quite high for each region, as seen by the small value of σ_1 and σ_2 in $D(\mu)$. The second-kind disorder of the $\mathbf{a}_2$ vector, g_{2j} (j = 1, 2), is small for both polymers. There is a slight difference in disorder with direction: g_{21} is smaller than g_{22}, which indicates that while the bilayer shows very little undulation, and that there is some variability in the separation distance of the R_f groups in the layer. The disorder of $\mathbf{a}_1$ in the $\mathbf{a}$ direction (x-axis), g_{11}, is also small, which indicates that disorder in the thickness of the layer is small. The disorder of $\mathbf{a}_1$ in the $\mathbf{b}$ and $\mathbf{c}$ directions, g_{22}, is larger than 0.5 in each case (Figure 8c). This disorder is responsible for the long-streak shape of the lateral (010) or (001) diffractions, and indicates that there is almost no positional correlation in the yz-direction between R_f groups in neighboring layers. These 2D crystal-like features are expected for the hexatic smectic phase (Figure 8d). Unfortunately, additional hkl diffractions[41] could not be obtained, and we were unable to determine whether the smectic phase was smectic-F or smectic-I. If one were able to fabricate a well-oriented fiber with 001 or 011 reciprocal vectors aligned perpendicular to the fiber axis, it would be possible to obtain quasi-hexagonal-symmetric diffraction patterns and explicitly determine the tilting direction and identify the smectic phase.[42]

The GI-WAXD results reveal that the PFA-C_8 and PFAVE8 form similar tilted hexatic phases. Simulations for the WAXD patterns in the Born approximation using the paracrystal model show that almost no correlation exists between the neighboring layers, which is expected for 2D crystals. The disordered 2D-crystal like features of the polymers are characteristic of the hexatic smectic phase.[43] The nearly identical phase structure of the polymers is consistent with the small difference in transition entropy observed with DSC.

3.5. FTIR Measurement to Determine the Molecular Orientation. The FTIR spectra of the powder and thin-films are shown in Figure 9. The orientation direction of functional groups (C═O in PFA-C_8 and −CH_2− in PFA-C_8 and PFVE8) was evaluated by comparing perpendicularly oriented thin-films to the nonoriented powder samples. Oriented thin-films with R_f chains aligned almost perpendicular to the surface were prepared by dip-coating on KBr plate. The dip-coated thin film showed similar orientation to the spin coated film, which is consistent with the prior report by Matsunaga et al.[44] The bands at 1148 and 1202 cm^{-1}, which correspond to the CF_2 symmetric and asymmetric vibration modes, respectively, were used to normalize the FTIR spectrum for the oriented and nonoriented samples. The transition moments of these vibration modes are perpendicular to the long-axis of the R_f chains. The GI-WAXD measurements discussed in the previous section show that the long-axis is tilted with respect to the surface normal by approximately 8° for PFA-C_8 and 12° for PFAVE8, which corresponds to the volume-averaged values of the orientation angle, μ_i, in section 3.4. Since the absorbance of infrared radiation is proportional to $\langle \sin^2\theta \rangle$, where θ is the angle between the direction of the transition moment and the normal to the surface (see SI),[45,46] the ratio of the absorbance of the orientated thin film to the powder may be defined by $\langle \sin^2\theta \rangle / \langle \sin^2\theta_0 \rangle$. The angle between the transition moment of the CF_2 symmetric vibration mode and surface normal directions, θ_0, is $(90 - 8)° = 82°$ and $(90 - 12)° = 78°$ for PFA-C_8 and PFAVE8, respectively. On the basis of the stretching band at 1737 cm^{-1}, the orientation of the carbonyl group in PFA-C_8 may be estimated as about 40° with respect to the surface normal. The estimated orientation angle from the in-plane absorbance and θ_0 is consistent with the previously reported value of 37°, which was directly estimated from out-of-plane and in-plane absorbance by Matsunaga et al.[44] The agreement between orientation angles indicates that the degree of orientation is the same in spin-coated and dip-coated films.

Symmetric and asymmetric CH_2 stretching bands were observed at 2930 and 2970 cm^{-1} in PFA-C_8 powder and at 2885 and 2920 cm^{-1} in PFAVE8 powder, respectively. For the PFAVE8, the powder and oriented thin films show large absorbance peaks of similar magnitude, while for the PFA-C_8, the absorbance of the oriented thin film is significantly diminished ($<\sin^2\theta>/<\sin^2\theta_0> < 0.1$ for the symmetric CH_2 stretching band). The ratios of the absorbance of the thin film to the powder were 0.9 and 0.6 for the bands at 2885 and 2920 cm^{-1} in PFAVE8. Considering that the transition moments of these bands are perpendicular to the long-axis of the dimethylene spacer, the absorbance ratio of thin film to powder for the CH_2 symmetric stretching band will be proportional to $\langle \sin^2(\theta_s + \pi/2) \rangle$, where θ_s is the angle between the long axis of CH_2 and surface normal. For the PFA-C_8, θ_s is near 90°, while for the PFAVE8, θ_s is near 0°. The FTIR results indicate that the −CH_2CH_2− spacer in PFA-C_8 tends to lie in the same yz-plane (surface) as the backbone chain. This model is consistent with that proposed by Matsunaga et al.[44] In contrast, for the PFAVE8, the spacer tends to align perpendicular to the yz-plane.

One probable molecular model for the atactic-like 5-mer of PFA-C_8 and PFAVE8 with "$mrmr$" tacticity (m: meso, r: racemo) that satisfies the orientation of the dimethylene spacer and R_f

dx.doi.org/10.1021/ma500503z | Macromolecules 2014, 47, 3860−3870

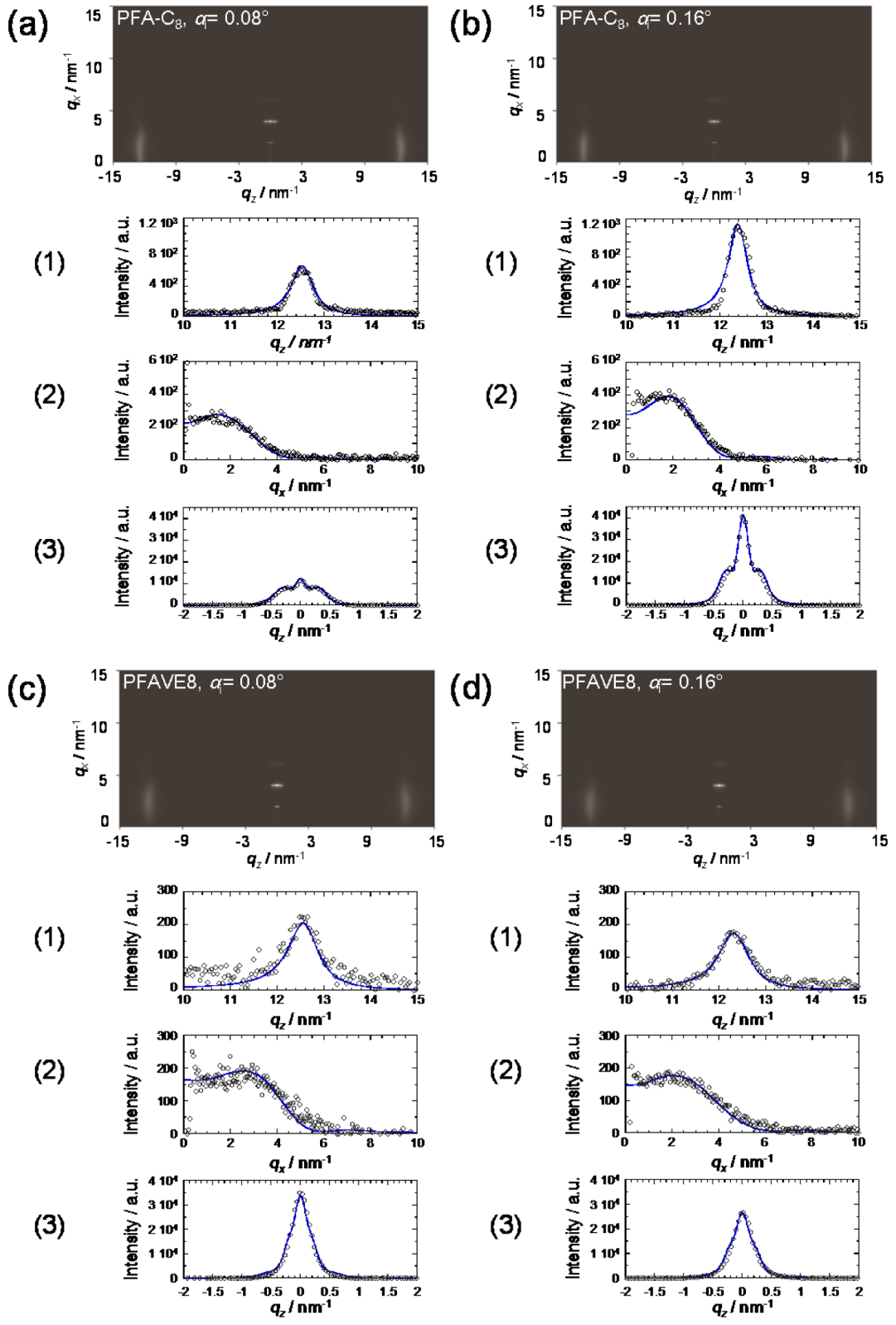

Figure 7. Simulated 2D-WAXD images in Born approximation; PFA-C_8 with (a) $\alpha_i = 0.08°$ and (b) 0.16° and PFAVE8 with (c) $\alpha_i = 0.08°$ and (d) 0.16°. The observed (open circles) and calculated (solid line) line intensity profiles corresponding to scattering vectors of (1) $q_x = 0$, (2) $q_z = c^*/2\pi$ (vertical line), and (3) $q_x = 2a^*/2\pi$ (horizontal line) are shown below each image.

chains estimated above is shown in Figure 10. In the model for PFA-C_8, the R_f mesogens must be projected to one side of the backbone chain to avoid steric repulsion between the backbone and the dimethylene spacer, which has long-axis almost parallel to the *yz*-plane. In other words, the geometric constraints force the long-axes to be, on average, parallel to the plane containing the polymer backbone. The oxygen atoms are concentrated around the backbone and the carbonyl dipoles in the upper and

dx.doi.org/10.1021/ma500503z | *Macromolecules* 2014, 47, 3860−3870

Table 1. Parameters Used for 2D GI-WAXD Simulation

incident angle/deg	a/nm[a]	b/nm[b]	δ/deg[c]	g_{11}[d]	g_{12}[e]	g_{21}[f]	g_{22}[g]	μ_1/deg[h,i]	μ_2/deg[h,i]	σ_1/deg[j,k]	σ_2/deg[j,k]	f_1[l,m]	f_2[l,m]
						PFA-C_8							
0.08	3.2	0.51	12	0.05	>0.5	0.09	0.02	12	5	1	2	0.5	0.5
0.16	3.2	0.51	11	0.05	>0.5	0.09	0.02	11	5	1	2	0.5	0.5
						PFAVE8							
0.08	3.1	0.52	16	0.05	>0.5	0.1	0.01	16	10	1	1	0.5	0.5
0.16	3.1	0.52	15	0.05	>0.5	0.1	0.01	15	9	1	1	0.6	0.4

[a]Lattice parameter along long-axis of mesogen. [b]Lattice parameter in layer plane (c-direction). [c]Tilt angle of hexatic phase (angle between layer normal direction and mesogen long-axis). [d]Standard deviation of a in a-direction. [e]Standard deviation of a in b-direction. [f]Standard deviation of b in a-direction. [g]Standard deviation of b in b-direction. [h,i]Orientation angle between a-axis and surface normal (x-axis) direction in regions 1 and 2, respectively. [j,k]Standard deviations of orientation angles, μ_1 and μ_2, respectively. [l,m]Volume fractions of regions 1 and 2, respectively.

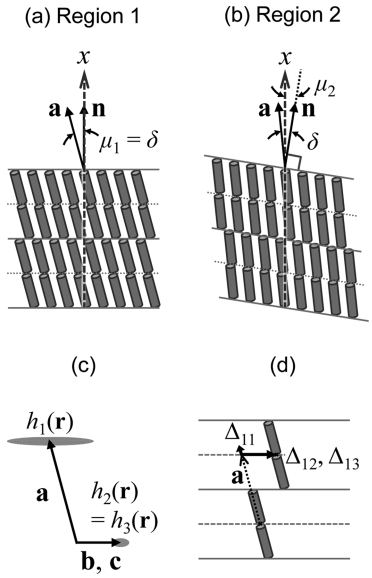

Figure 8. Schematic models showing the orientation of the tilted hexatic phase: (a) region 1 and (b) region 2. The direction of **a** vector and layer normal direction (**n**) are shown by arrows. (c) Schematic illustration showing distribution of lattice vectors $\mathbf{a}_k$, $h_k(\mathbf{x})$. (d) Correlation between the R_f groups in neighboring layers. Standard deviation of $\mathbf{a}_1$ in the **b** and **c** direction (Δ_{12}, Δ_{13}) is much larger than that in **a** direction (Δ_{11}). The vectors **a**, **b**, **c** represent $\langle \mathbf{a}_1 \rangle$, $\langle \mathbf{a}_2 \rangle$, $\langle \mathbf{a}_3 \rangle$, which are statistically averaged values of lattice vectors.

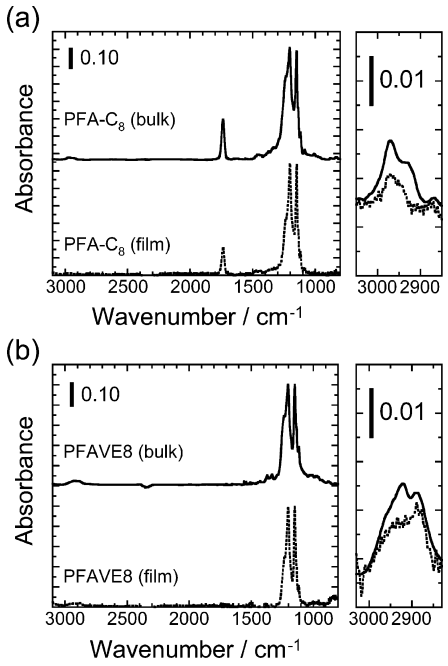

Figure 9. Transmission mode FTIR spectrum: (a) PFA-C_8 and (b) PFAVE8. Solid and dotted lines correspond to measurements of the powder sample and dip-coated thin films on KBr substrate, respectively. The spectra are normalized by the CF_2 symmetric vibration band at 1148 cm^{-1}. Magnified spectra around 2900 cm^{-1} are shown on the right.

lower chains must be nearly antiparallel to each other, as discussed in section 3.2.

In the model for PFAVE8, the oxygen atoms are projected to both sides of the backbone and the transition moment of the asymmetric stretching vibration of the backbone CH_2 tends to align perpendicular to the yz-plane. In other words, the long axis of R_f groups is perpendicular to the dihedral plane of C−C bonds in the backbone. In contrast to the PFA-C_8, if the dimethylene spacers are projected to one side, it is difficult to satisfy the condition that both R_f groups and the dimethylene spacer are parallel in the x-axis direction within three rotational-isomeric states. Consequently, the oxygen atoms will be concentrated near the backbone for PFA-C_8 while for the PFAVE8, they are distributed above and below the backbone, as shown in Figure 10. The distribution of oxygen atoms in these models are in agreement with the electron density profile in Figure 3c. Attractive interactions between polymer backbones will not be favored in this conformation for the PFAVE8. The difference in the linkage between the backbone and spacer is therefore responsible for such significant differences in preferred conformation.

The FTIR results reveal that although the PFA-C_8 and PFAVE8 form similar tilted hexatic phases, the direction of spacer groups is different. The spacer direction dominates the manner in which the R_f chains are projected from the backbone and determines the alignment of polar groups. The polar group orientation significantly affects the interchain interactions and thereby influences transition enthalpy and isotropization temperature.

3.6. Discussion. The objective of this work has been to elucidate the structural mechanisms responsible for the significant difference in isotropization temperature PFA-C_8 (79 °C) and PFAVE8 (29.5 °C). Both polymers form similar tilted hexatic phases and have nearly identical transition entropies, ΔS, which indicates that the difference in transition temperature must depend on transition enthalpy, ΔH. Despite similar structural features between the R_f groups and n-alkyl side-chain polymers, the observed thermal behavior is opposite that reported for series of poly(n-alkyl acrylate)s and poly(n-alkyl acrylate)s.[1] WAXD measurements show that the ordered structure of the polymers investigated here is not affected by the polymer backbone and

dx.doi.org/10.1021/ma500503z | Macromolecules 2014, 47, 3860−3870

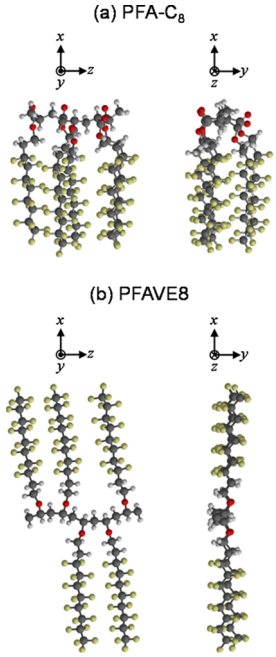

Figure 10. 3D molecular model of 5-mer with *mrmr* (*m*, meso; *r*, racemo) tacticity for (a) PFA-C_8 and (b) PFAVE8. The orientation of the functional groups, paticularly the dimethylene spacer, corresponds to FTIR measurements. Cartesian coordinates inset above the model.

that the ordering behavior of R_f side chains at the surface is similar to *n*-alkyl side-chain polymers.[6] The results indicate that the difference in T_i cannot be explained by differences in the primary structures or in the liquid-crystalline structure. Therefore, it is anticipated that the conformation, which does not affect the liquid-crystalline structure, is responsible for the differences in ΔH and T_i.

FT-IR measurements discussed in section 3.5 indicate that the R_f side chains are projected on one side from the backbone for PFA-C_8 and on both sides from the backbone for PFAVE8. Assuming that there is no interdigitation between chains in neighboring layers, the layer spacing calculated from the proposed molecular model in Figure 10 is 3.24 nm (=2 × 16.5 nm × cos 11°) for PFA-C_8 and 3.04 nm (=31.6 nm × cos16°) for PFAVE8. These values are in good agreement with the estimated values from the WAXD measurements. Moreover, the WAXD results revealed that the lateral distance between R_f groups and degree of disorder of the lattice are almost the same for the two polymers. It can then be concluded that the effect of R_f group is small and negligible for these polymers and that the difference in ΔH is due to the difference in interactions between non-R_f groups, i.e., carbonyl groups in PFA-C_8 and ether groups in PFAVE8. In the proposed molecular model, the oxygen atoms in PFA-C_8 are concentrated around the backbone and the carbonyl dipoles in the upper and lower chains show favorable interactions and permit stacking in a nearly antiparallel arrangement. The distribution of the oxygen atoms in these models are in agreement with the electron density profile in Figure 3c obtained from powder WAXD.

From the above discussion, it may be concluded that the difference in conformation has little influence on ΔS. The results indicate that the packing (translational) entropy of the mesogen dominates ΔS in the highly ordered smectic phases. In the case of the hexatic smectic phase, the backbone chains must be significantly constrained between the smectic layers to accommodate the 2D hexagonal lattice and therefore will have few degrees of freedom. As a result, the backbone conformation may not affect ΔS. This suggests that similar values of ΔS may also be expected for other side-chain polymers that form highly ordered phases with similar structure.

Previously, the number of carbon atoms in the fluoroalkyl side chains has been regarded as the critical factor responsible for the surface properties of fluorinated side-chain polymers because it determines whether the polymer can form an ordered phase. Here, the type of linkage is found to dominate the thermal tolerance of the ordered phase (isotropization temperature), which is an important factor in the design of practical materials.

4. CONCLUSION

Comb-shaped polymers with fluorooctyl ethyl side-chains connected on poly(acrylate) (PFA-C_8) and poly(vinyl ether) backbones (PFAVE8) were prepared and show large differences in the isotropization temperature, T_i (79 °C for the PFA-C_8 and 29.5 °C for the PFAVE8). Structural analysis based on synchrotron-source X-ray diffraction showed that these polymers form the same tilted hexatic smectic phase with similar levels of disorder. The mechanism of ordered phase formation and growth appears to be the same for the two polymers, although the electron density around the PFA-C_8 backbone is larger than that of the PFAVE8. FTIR measurements of perpendicularly oriented thin films revealed that the orientation of the dimethylene spacer group is different between the two polymers. The difference in spacer orientation results in geometric constraints that influence how the R_f chains are projected from the backbone. The R_f chains are projected to only one side in the PFA-C_8, while for the PFAVE8, the R_f chains are projected to both sides. The large difference in transition enthalpy and isotropization temperature is attributed to the higher concentration of polar carbonyl groups around the backbone for the PFA-C_8, which increases the magnitude of interchain interactions. The results show that in addition to the length of the R_f group, the type of linkage between the polymer backbone and the mesogenic R_f chains is an important factor that must be considered in the design of thermally tolerant fluorinated comb-shaped polymers.

■ ASSOCIATED CONTENT

Ⓢ Supporting Information

Powder WAXD raw (nonintegrated) profiles for PFA-C_8 from 27 to 85 °C, detailed derivation and calculation processes for electron density distribution in the layer normal direction (section 3.2), GI-WAXD pattern (section 3.4), and relationship between orientation angle and IR absorbance (section 3.5). This material is available free of charge via the Internet at http://pubs.acs.org.

■ AUTHOR INFORMATION

Corresponding Author

*(A.T.) Telephone: +81-92-802-2517. Fax: +81-92-802-2518. E-mail: takahara@cstf.kyushu-u.ac.jp.

Notes

The authors declare no competing financial interest.

■ ACKNOWLEDGMENTS

The authors thank Unimatec Co. Ltd, Ibaraki, Japan for providing FAVE8. Synchrotron wide-angle X-ray powder diffraction (WAXD), microbeam WAXD and grazing-incidence WAXD (GI-WAXD) measurements were conducted on the BL02B2, BL40XU and BL03XU beamlines in SPring-8, respectively, with the approval of the Japan Synchrotron

Radiation Research Institute (JASRI). The proposal numbers were 2012B1234 (BL02B2) and 2012A1291 (BL40XU). We thank Dr. Jungeun Kim, Dr. Noboru Ohta, and Dr. Hiroki Ogawa for experimental assistance on the BL02B2, BL40XU, and BL03XU beamlines, respectively. We also gratefully acknowledge Dr. Kazuki Mita (Mitsui Chemicals, Inc.) for kindly giving us an opportunity to conduct thin film WAXD measurements at the BL03XU.

REFERENCES

(1) Platé, N. A.; Shibaev, V. P. *J. Polym. Sci.: Macromol. Rev.* **1974**, *8*, 117−253.
(2) Linford, M. R.; Feter, P.; Eisenberger, P. M.; Chidsey, C. E. D. *J. Am. Chem. Soc.* **1995**, *117*, 3145−3155.
(3) Roussel, F.; J Buisine, J.; Maschke, U.; Coqueret, X.; Benmouna, F. *Phys. Rev. E* **2000**, *62*, 2310−2316.
(4) Roussel, F.; Fung, B. *Phys. Rev. E* **2003**, *67*, 041709.
(5) Gautam, K. S.; Dhinojwala, A. *Macromolecules* **2001**, *34*, 1137−1139.
(6) Gautam, K. S.; Dhinojwala. *Phys. Rev. Lett.* **2002**, *88*, 145501.
(7) Rangwalla, H.; Schwab, A. D.; Yurdumakan, B.; Yablon, D. G.; Yeganeh, M. S.; Dhinojwala, A. *Langmuir* **2004**, *20*, 8625−8633.
(8) Doi, T.; Sakurai, Y.; Tamatani, A.; Takenaka, S.; Kusabayashi, S.; Nishihata, Y.; Terauchi, H. *J. Mater. Chem.* **1991**, *1*, 169−173.
(9) Pées, B.; Sindt, M.; Paul, J. M.; Mieloszynski, J. L. *Eur. Polym. J.* **2002**, *38*, 921−931.
(10) Shimizu, T.; Tanaka, Y.; Kutsumizu, S.; Yano, S. *Macromol. Symp.* **1994**, *82*, 173−184.
(11) Shimizu, T.; Tanaka, Y.; Kutsumizu, S.; Yano, S. *Macromolecules* **1996**, *29*, 156−164.
(12) Galli, G.; Gasperetti, S.; Bertolucci, M.; Gallot, B.; Chiellini, F. *Macromol. Rapid Commun.* **2002**, *23*, 814−818.
(13) Martinnelli, E.; Paoli, F.; Gallot, B.; Galli, G. *J. Polym. Sci., Part A: Polym. Chem.* **2010**, *48*, 4128−4139.
(14) Zaggia, A.; Ameduri, B. *Curr. Opin. Colloid Interface Sci.* **2012**, *17*, 188−195.
(15) de Gennes, P. G.; Prost, J. In *The Physics of Liquid Crystals*; de Gennes, P. G., Prost, J., Eds.; Oxford University Press: New York, 1995; p 22−24.
(16) Volkov, V. V.; Platé, N. A.; Takahara, A.; Kajiyama, T.; Amaya, N.; Murata, Y. *Polymer* **1992**, *33*, 1316−1320.
(17) Corpart, J.-M.; Girault, S.; Juhué, D. *Langmuir* **2001**, *17*, 7237−7244.
(18) de Crevoisier, G.; Fabre, P.; Leibler, L.; Tencé-Girault, S.; Corpart, J. M. *Macromolecules* **2002**, *35*, 3880−3888.
(19) Honda, K.; Yakabe, H.; Koga, T.; Sasaki, S.; Sakata, S.; Otsuka, H.; Takahara, A. *Chem. Lett.* **2005**, *34*, 1024−1025.
(20) Honda, K.; Yamaguchi, Y.; Sakata, O.; Sasaki, S.; Takata, M.; Morita, M.; Takahara, A. *J. Phys: Conf. Ser.* **2009**, *184*, 012007(1)−(4).
(21) Honda, K.; Morita, M.; Otsuka, H.; Takahara, A. *Macromolecules* **2005**, *38*, 5699−5705.
(22) Yamaguchi, H.; Kikuchi, M.; Kobayashi, M.; Ogawa, H.; Masunaga, H.; Sakata, O.; Takahara, A. *Macromolecules* **2012**, *45*, 1509−1516.
(23) Höpken, J.; Möller, M.; Lee, M.; Percec, V. *Makromol. Chem.* **1992**, *193*, 275−284.
(24) Meskini, A.; Raihane, M.; Ameduri, B. *Macromolecules* **2009**, *42*, 3532−3539.
(25) Ameduri, B. Boutevin, B. In *Well-Architectured Fluoropolymers: Synthesis, Properties and Applications*; Elsevier: Amsterdam, 2004; pp 187−222.
(26) Muroyama, N.; Ohsuna, T.; Ryoo, R.; Kubota, Y.; Terasaki, O. *J. Phys. Chem. B* **2006**, *110*, 10630−10635.
(27) Ogawa, H.; Masunaga, H.; Sasaki, S.; Goto, S.; Tanaka, T.; Seike, T.; et al. *Polym. J.* **2013**, *45*, 109−116.
(28) Omenat, A.; Lub, J.; Fischer, H. *Chem. Mater.* **1998**, *10*, 518−523.
(29) Ishige, R.; Yamaguchi, H.; Shinohara, T.; Meskini, A.; Raihane, M.; Takahara, A.; Ameduri, B. *Polym. J.* **2013**, *45*, 1041−1046.
(30) Kasai, N.; Kakudo, M. In *X-ray Diffraction by Macromolecules (Springer Series in Chemical Physics)*; Kodansha Ltd. and Springer-Verlag: Tokyo, 2005; Chapter 11, p 289.
(31) Roe, R.-J. In *Methods of X-ray and Neutron Scattering in Polymer Science*; Oxford University Press: New York, 2000; Chapter 3, p 90.
(32) Shoji, Y.; Ishige, R.; Higashihara, T.; Morikawa, J.; Hashimoto, T.; Takahara, A.; Watanabe, J.; Ueda, M. *Macromolecules* **2013**, *46*, 747−755.
(33) Kasai, N.; Kakudo, M. In *X-ray Diffraction by Macromolecules (Springer Series in Chemical Physics)*; Kodansha Ltd. and Springer-Verlag: Tokyo, 2005; Chapter 10, pp 239−271.
(34) Ocko, B. M.; Braslau, A.; Pershan, P. S.; Als-Nielsen, J.; Deutsch, M. *Phys. Rev. Lett.* **1986**, *57*, 94−97.
(35) Omote, K.; Ito, Y.; Kawamura, S. *Appl. Phys. Lett.* **2003**, *82*, 544−546.
(36) Babonneau, D. *J. Appl. Crystallogr.* **2010**, *43*, 929−936.
(37) Guinier, A. In *X-ray Diffraction In Crystals, Imperfect Crystals, and Amorphous Bodies*; W. H. Freeman and Company: San Francisco, CA, 1963, Chapter 9, p 295−317.
(38) Hosemann, R.; Baguchi, S N. In *Direct Analysis of Diffraction by Matter*; North-Holland: Amsterdam, 1962; Chapter 9, p 302−353.
(39) Wilke, W. *Acta Crystallogr.* **1983**, *A39*, 864−867.
(40) Hashimoto, T.; Kawamura, T.; Harada, M.; Tanaka, H. *Macromolecules* **1994**, *27*, 3063−3072.
(41) Tokita, M.; Okuda, S.; Yoshihara, S.; Takahashi, C.; Kang, S.; Sakajiri, K.; Watanabe, J. *Polymer* **2012**, *53*, 5596−5599.
(42) Gallot, B.; Galli, G.; Ceccanti, A.; Chiellini, E. *Polymer* **1999**, *40*, 2561−2568.
(43) Chandrasekhar, S. In *Liquid Crystals*, 2nd ed.; Cambridge University Press: Cambridge, U.K., 1992; p 360.
(44) Matsunaga, M.; Suzuki, T.; Yamamoto, K.; Hasegawa, T. *Macromolecules* **2008**, *41*, 5780−5784.
(45) Stein, R. S. *J. Polym. Sci.* **1958**, *31*, 327−334.
(46) Read, B. E.; Stein, R. S. *Macromolecules* **1967**, *1*, 116−126.